Understanding Transport Barriers through Modeling

V. Rozhansky

St.-Petersburg State Polytechnical University,

Polytechnicheskaya 29 Russia

Main concepts of the barrier formation

At present it is well understood that the key element in the transition physics is the origin of the strong radial electric field and suppression of the turbulence fluctuation level by a strong poloidal rotation in the $\vec{E}\times\vec{B}$ fields. As a result, the transport coefficients are strongly reduced at fixed places and transport barriers with steep density and temperature gradients are formed near the separatrix or last closed flux surface (ETB) or in the core region (ITB). The key element in the transition physics is the origin of the strong radial electric field. The mechanisms may be separated into three main groups.

i. Bifurcation models

Based on the old idea of Stringer that in the neoclassical theory several solutions for the radial electric field may exist for the same set of plasma parameters.

Many authors have studied this possibility and it was demonstrated that besides the normal poloidal rotation, which should be of the order of T_i / eBL_n, $(L_n = (d\ln n / dr)^{-1})$ the other solutions with the poloidal rotation velocity of the order of the poloidal sound speed exist. The possibility of multiple solutions has been invoked to explain the L-H transition mechanism by Itoh and Itoh and Shaing and Crume in 1989.

Shaing suggested the combination of orbit-loss current, which is caused by the particles crossing the separatrix and current driven by non-linear parallel viscosity, as bifurcation mechanism.

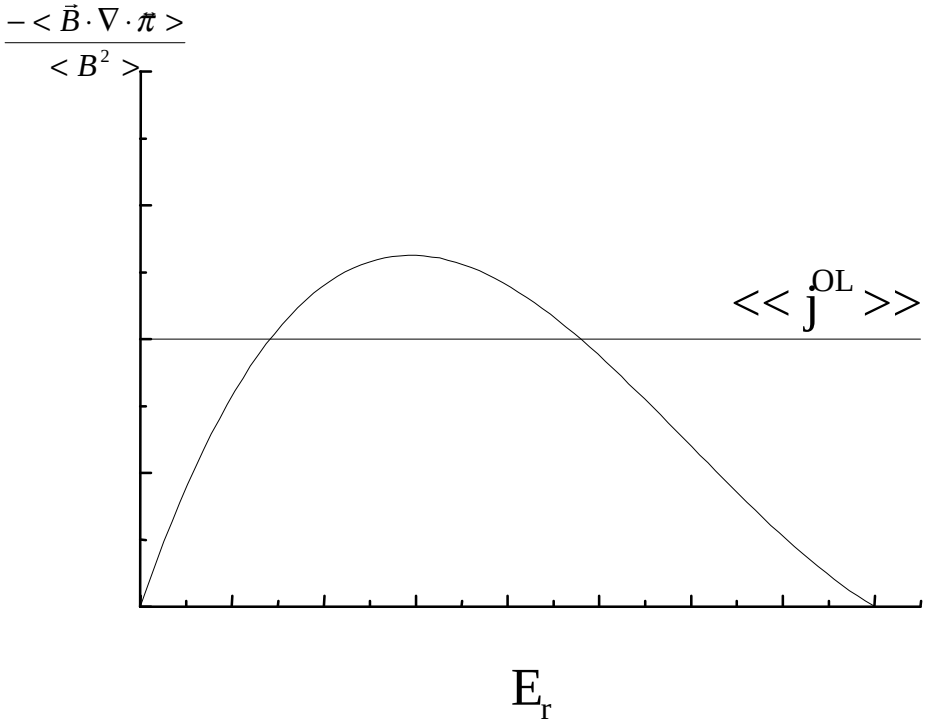

Fig.1 Orbit-loss radial current (horizontal line) is balanced by the radial current driven by the parallel viscosity, which depends non-lineary on the radial electric field. Two solutions for electric field are predicted.

In these early approaches important effects connected with the anomalous transport, especially momentum transport, were ignored. From the point of experiment this model cannot predict the observed L-H transition in the high collisionality regime, when the loss-orbit current is low. The poloidal rotation, which should be of the order of the poloidal sound speed, also contradicts the experiment, where the radial electric field is determined by the density and temperature gradients.

ii. Spin-up mechanism

In the other group of theories (Hassam et al. 1991, Diamond et al. 1994 and others) the mechanism of spin up in the poloidal rotation by the plasma turbulence was suggested. In contrast to the previous group, the turbulent processes were analyzed but either only part of the toroidal effects were taken into account or the pure cylindrical approximation was considered and all the neoclassical effects were neglected.

In other words such an analysis may predict the effective anomalous viscosity (Reynolds stress tensor) and other anomalous transport coefficients, **however to obtain radial electric field, poloidal and toroidal rotations one has to solve the full set of particle and momentum balance equations with all the toroidal effects.**

iii. Neoclassical radial electric field in combination with anomalous transport

The radial electric field is determined by the momentum balance equations including both neoclassical effects and anomalous terms. Rozhansky and Tendler 1992 demonstrated that radial electric field **is close to the neoclassical value** at least for not too steep density and temperature profiles.

In contrast to the standard neoclassical theory the **toroidal rotation** velocity is mainly determined by **anomalous transport of the parallel (toroidal) momentum**.

The radial electric field shows no bifurcation and the origin of the strong electric field in the H-mode might be explained by the self-consistent change of the plasma profile.

Analytical model for radial electric field

To predict poloidal and toroidal rotations it is necessary to analyze two equations.

Parallel momentum balance

$$-b_x \frac{\partial p}{h_x \partial x} - (\nabla \cdot \vec{\pi}_{\|})_{\|} + F^{(ex)} = \frac{d(m_i n V_{\|})}{dt}, \qquad (1)$$

where

$$\frac{d(m_i n V_{\|})}{dt} = \frac{1}{h_z \sqrt{g}} \frac{\partial}{\partial y} \left[\frac{h_z \sqrt{g}}{h_y} \left(m_i \Gamma_y V_{\|} - \frac{\eta}{h_y} \frac{\partial V_{\|}}{\partial y} \right) \right] . \qquad (2)$$

Here Γ_y is the radial particle flux: $\Gamma_y = -D \frac{\partial n}{h_y \partial y} + Vn$ with D and V being the anomalous coefficients of diffusion and convection, and η is the anomalous viscosity coefficient. The x and y co-ordinates correspond to the directions along and across flux surfaces accordingly, z is the toroidal direction, $h_{x,y,z}$ are metric coefficients, $b_x = B_x/B$, $b_z = B_z/B$.

The surface averaged parallel momentum balance equation

$$-\left\langle \vec{B} \cdot \nabla \cdot \vec{\pi}_{\|} \right\rangle + \left\langle \vec{B} \cdot \vec{F}^{(ex)} \right\rangle = \left\langle B n m_i \frac{dV_{\|}}{dt} \right\rangle . \qquad (3)$$

The standard neoclassical expression for the parallel viscosity

$$\left\langle \vec{B}\cdot\nabla\cdot\pi_{\parallel}\right\rangle = -\nu^{(mp)} n m_i \left(\frac{B}{h_y B_x}\left(\frac{\partial\varphi}{\partial y} + \frac{T_i}{en}\frac{\partial n}{\partial y} + k_T \frac{\partial T_i}{e\partial y}\right) - \left\langle BV_z\right\rangle \right). \qquad (4)$$

The magnetic pumping frequency $\nu^{(mp)}$ and coefficient $k^{(T)}$ depend on collisionality.

As a second equation it is convenient to use the toroidal component of the momentum balance equation. Resolving it one obtains the surface averaged radial current density through the flux surface

$$\left\langle\left\langle j_y\right\rangle\right\rangle = \left\langle\left\langle \frac{1}{B_x}\left[F^{(ex)} - m_i n \frac{dV_z}{dt}\right]\right\rangle\right\rangle \quad . \qquad (5)$$

To obtain the radial electric field profile one has to combine Eqs. (3) and (5). Radial electric field depends on the parameter

$$\kappa = \frac{\nu^{(mp)} L^2}{D} \quad , \qquad (6)$$

where L is the density or temperature spatial scale. If $\kappa >> (r/R)^2$, which is typical for the core region, the radial electric field is given by the condition $\left\langle \vec{B}\cdot\nabla\cdot\pi_{\parallel}\right\rangle = 0$ and coincides with the neoclassical expression

$$E^{(NEO)} = \frac{T_i}{e}\left(\left(\frac{1}{h_y}\frac{d\ln n}{dy} + k_T \frac{1}{h_y}\frac{d\ln T_i}{dy}\right) - \frac{B_x}{B}\left\langle BV_z\right\rangle \right). \qquad (7)$$

However, near the separatrix, where the spatial scale L is significantly smaller, the parameter κ may be small and hence the radial electric field might be more complicated.

Simulation of the radial electric field in L-mode with 2D fluid codes

The fluid transport equations of Braginskii are widely used for simulation of the edge tokamak plasma in the transport codes such as B2, UEDGE, EDGE2D, TECXY, B2SOLPS5.0. In these codes the fluid equations are solved with perpendicular transport coefficients (diffusivity, heat conductivities, viscosity) being replaced by anomalous values. The radial electric field obtained by these codes show quite similar features.

1. **Radial electric field is negative in the core region near the separatrix and positive in the scrape-off layer** (Rognlien T D et al 1999, Rozhansky et al 2001, 2002, Gerhauser H et al 2002).
2. **Radial electric field inside the separatrix is close to the neoclassical electric field for wide set of plasma parameters** (Rozhansky et al 2002).

Example of simulation by B2SOLPS5.0 (Rozhansky et al 2002)

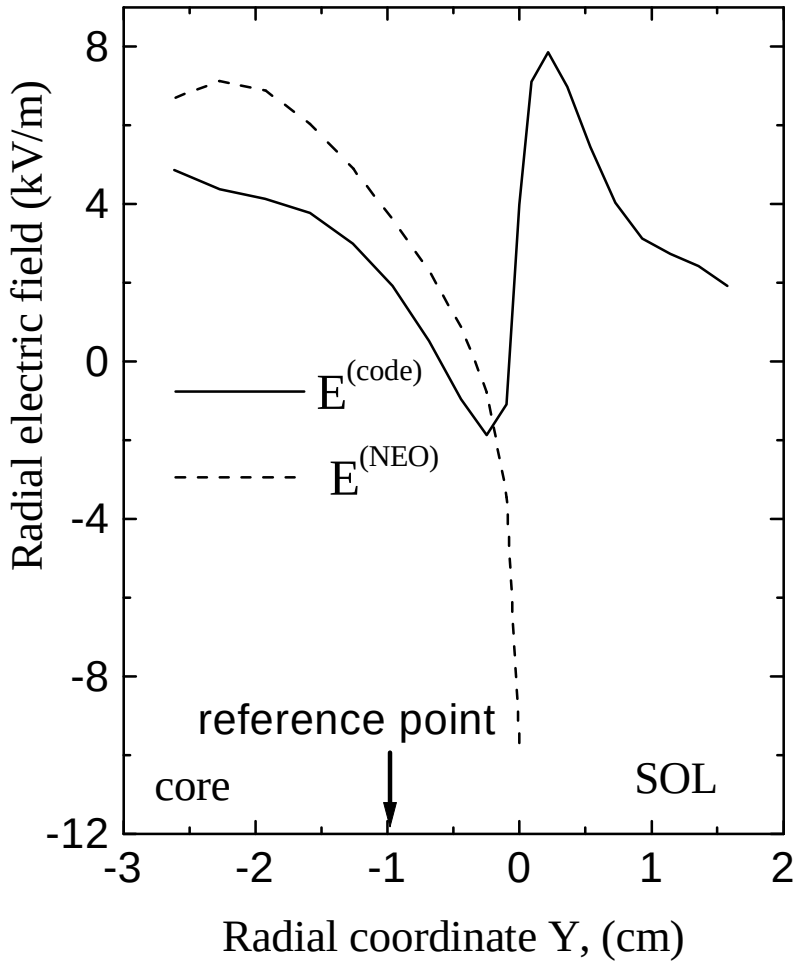

Fig.2a. Radial electric field in ASDEX Upgrade at the outer midplane for discharge with co-injection, normal direction of magnetic field, n=2·10^{19} m^{-3}, T_i=98 eV, $<V_{||}>$=-18 km/s in the reference point. I=1 MA, B=2 T.

Note, however, that the radial profile of the toroidal velocity is governed by anomalous radial transport and hence the radial electric field profile can not be predicted by standard neoclassical theory.

Another example

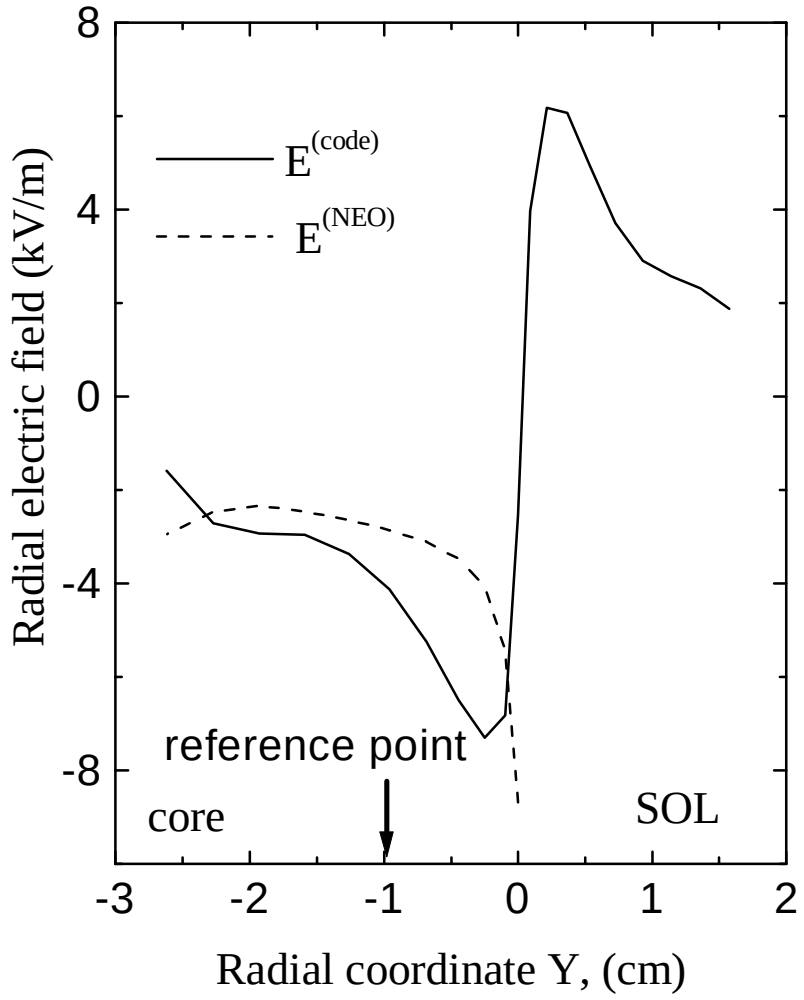

Fig. 2a. Radial electric field at the outer midplane for discharge without NBI, normal direction of magnetic field, n=2·10^{19} m^{-3}, T_i=98 eV in the reference point. I=1 MA, B=2 T.

In the vicinity of a separatrix the structure of the radial electric field is more complicated since the parameter κ becomes small and the role of anomalous transport of parallel momentum is amplified. Here the viscous layer exists which provides a transition from the core to the scrape-off layer (SOL). In this viscous layer the averaged parallel viscosity is balanced by the radial transport of the toroidal momentum. The width if this layer is (Rozhansky et al. 2002)

$$\delta \sim \left(\frac{B^2 a^2 D \nu_{ii}}{B_x^2 c_s^2} \right)^{1/2}, \qquad (8)$$

where c_s is the sound speed and a is the minor radius, ν_{ii} is the ion-ion collision frequency.

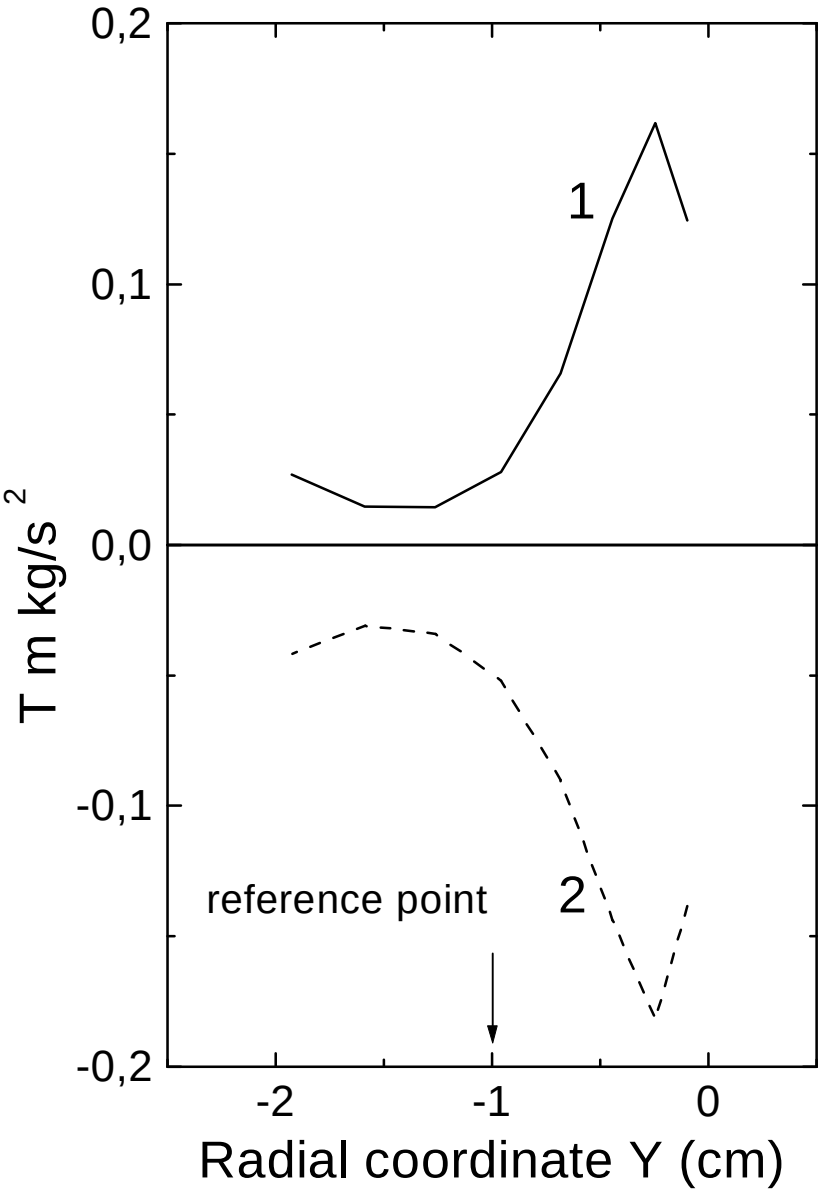

Fig. 3. Averaged parallel viscosity $\langle \vec{B} \cdot \nabla \cdot \boldsymbol{\pi}_{\parallel} \rangle$ 2, corresponding to the l.h.s. of parallel momentum balance Eq., and 1-the r.h.s. of this Eq. Both quantities decrease from the separatrix towards the core with the scale Eq. (8). Deeper in the core $\langle \vec{B} \cdot \nabla \cdot \boldsymbol{\pi}_{\parallel} \rangle \approx 0$ - neoclassical solution. The temperature scaling of the viscous layer width $\delta \sim T_i^{-5/4}$ is consistent with the simulation results.

Monte Carlo simulations of radial electric field

Fluid codes can predict the radial electric field for a collisional plasma when the collisionality parameter $\nu_{*i} > \varepsilon^{-3/2}$ (the flux limiting of the parallel transport may extend the applicability of fluid codes to the plateau regime $1 < \nu_{*i} < \varepsilon^{-3/2}$).

Monte Carlo code ASCOT (Heikkinen J A et al 2002) can produce results both low and high collisionality regimes. This code has some restrictions: it is impossible to simulate regimes with unbalanced NBI and obtain field outside the separatrix, where simplified boundary conditions are imposed. On the other hand, orbit loss effects, which are absent in the fluid codes, are automatically taken into account by ASCOT.

Results of the simulations of the Ohmic L-mode by ASCOT and B2SOLPS5.0 were compared (Kiviniemi T P et al 2003).

The two codes give similar results with the same viscosity coefficients.

Note that simulations with Monte Carlo code as well as with fluid codes do not predict any bifurcation of the electric field.

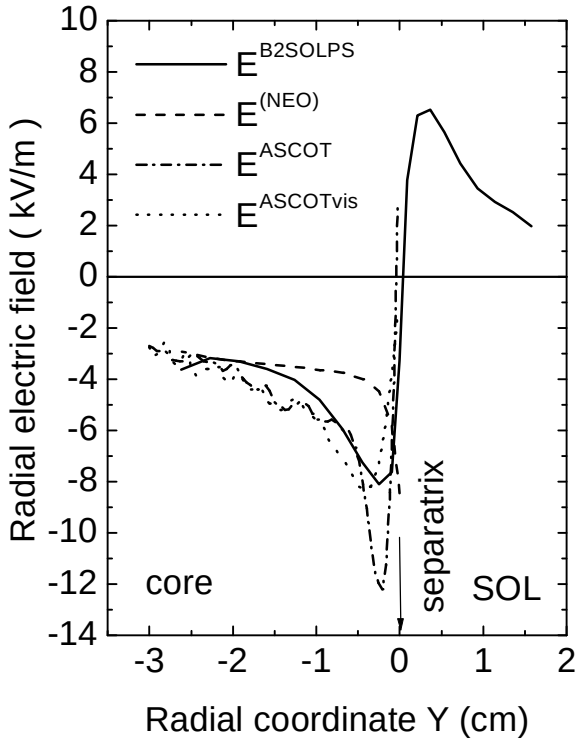

Fig.4. Comparison of simulations by B2SOLPS5.0 and ASCOT in the absence of NBI for ASDEX Upgrade, the separatrix temperature $T_i = 105eV$. The curve $E^{ASCOTvis}$ corresponds to the same anomalous viscosity as in B2SOLPS5.0.

Simulations of biasing experiments. Perpendicular conductivity

Critical test for our understanding of the radial electric field structure. Performed on several tokamaks (CCT, Taylor R J et al 1989, TUMAN-3, Askinazi L et al 1992, TEXTOR, Weynants et al 1992, and later on the others).

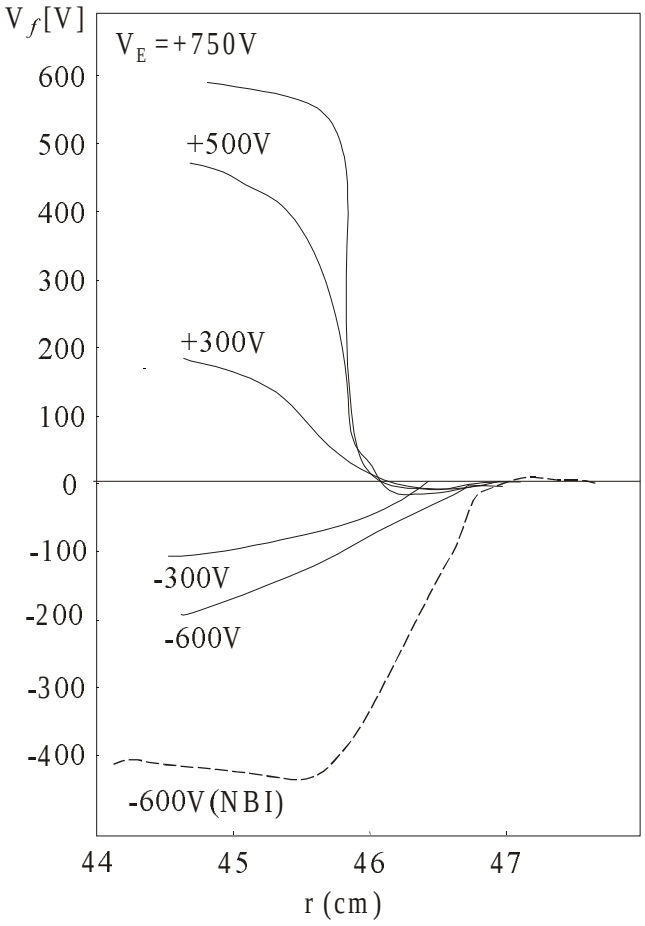

Fig.5. Radial profiles of floating potential measured for different applied voltages in the biasing experiment in TEXTOR.

The I-V characteristics and measured radial profile of the electric field should be explained theoretically thus providing understanding of the effective perpendicular conductivity in a tokamak and of the mechanisms responsible for the formation of the radial electric field.

It was demonstrated by Rozhansky et al, 2003, that the I-V characteristics as well as electric field profile during biasing might be understood on the base of equations (3)-(5). The analytical expressions for conductivity as well as the results of simulations by B2SOLPS5.0 are consistent with the data. Simulations of the biasing experiments were also performed by ASCOT, Heikkinen J A et al. 2000 and TECXY, Gerhauser H et al. 2002.

It was argued by Itoh K et al. 1998, Kasnya N et al. 2003, Kasnya N this workshop, that for large applied voltages the soliton-like solutions, where a narrow region of large electric field was localized somewhere between the biased electrode and the separatrix, might exist. However, the anomalous transport of toroidal momentum was not taken into account, therefore it remains unclear whether these effects exist in real experiments. No soliton formation was observed in the simulations.

Predictions for the L-H transition threshold. Comparison with experiment

In the simulations by B2SOPLS5.0 and ASCOT the parametric dependence of the radial electric field and its shear $\omega_s = \frac{RB_x}{B}\left|\frac{d(E_y / B_x R)}{h_y dy}\right|$ has been studied. The linear dependence of the shear on the local ion temperature and the local average toroidal velocity was obtained. The dependence on the density was found to be rather weak. Growth of electric field with heating power was reported by Rognlien T D et al 2000 (UEDGE).

Such dependencies are similar to what one can expect for the neoclassical electric field, Rozhansky et al 2002. Indeed, calculating the shear from Eq. (7), neglecting relatively small corrections (dB_x / dy, dB / dy, dR / dy), assuming linear profiles close to the separatrix with $L_T >> L_n$, where $L_n = \left|d \ln n / h_y dy\right|^{-1}$, $L_T = \left|d \ln T_i / h_y dy\right|^{-1}$, $L_V = \left|d \ln \langle V_\| \rangle / h_y dy\right|^{-1}$, $\langle V_\| \rangle \equiv \langle V_\| B \rangle / \langle B \rangle$, one obtains

$$\omega_s^{(NEO)} = \frac{1}{B}\left|\frac{T_i}{eL_n^2} - \frac{B_x}{L_V}\langle V_\| \rangle\right|. \qquad (9)$$

To predict the L-H transition threshold it is necessary to specify the critical shear when the transition may start. At present a robust model is still missing. Hence to perform comparison some value of the order of $10^5 s^{-1}$ may be chosen.

i. Normal magnetic field direction

In the simulations with B2SOPS5.0 for ASDEX Upgrade the critical shear the value $\omega_s = 3.5 \cdot 10^5 s^{-1}$ has been chosen. In the simulations with ASCOT $\omega_s = 5 \cdot 10^5 s^{-1}$ for ASDEX Upgrade and $\omega_s = 1.5 \cdot 10^5 s^{-1}$ for JET has been taken. It was demonstrated that to reach the chosen critical shear it is necessary to increase heating power proportionally to the local density and toroidal magnetic field.

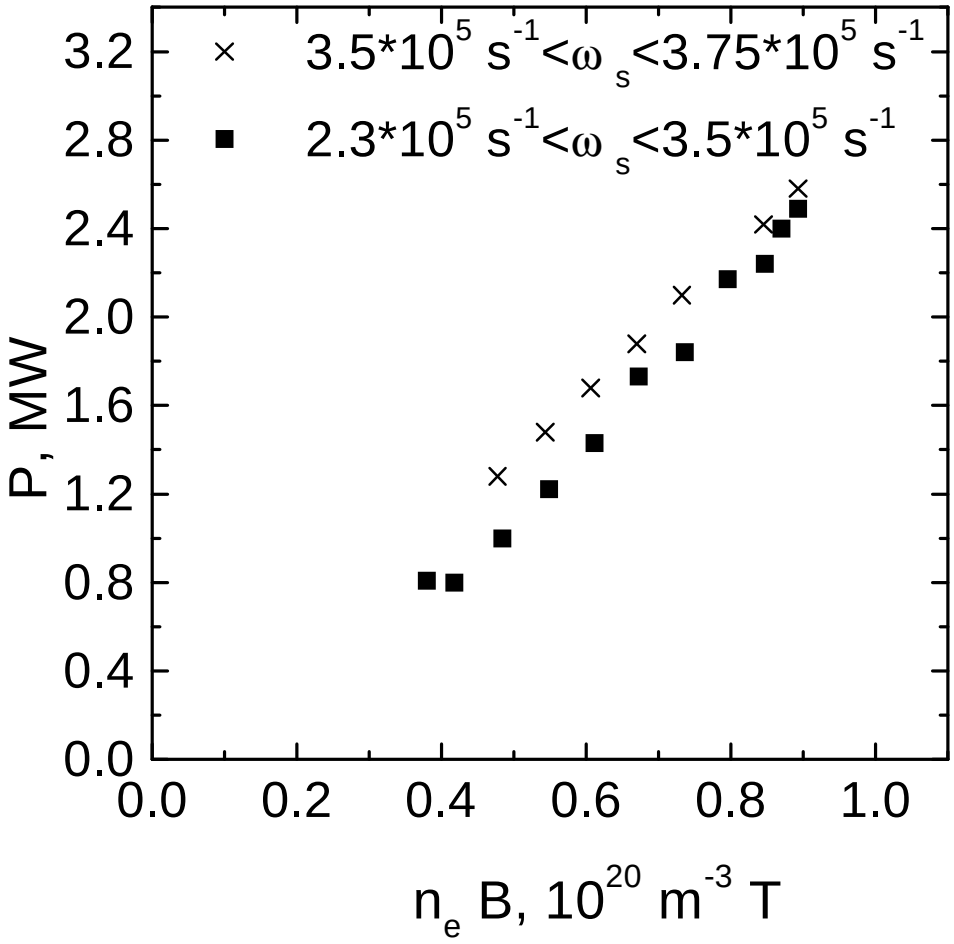

Fig.6a. Heating power which is necessary to achieve a given value of electric field shear (ω_s=3.5·10^5 s^{-1} at reference point) for ASDEX Upgrade for different plasma densities (at *r-a* = 2 cm). *I*=1 MA, *B*=2 T (Rozhansky et al 2002).

This is similar to the power threshold for ASDEX-Upgrade obtained experimentally.

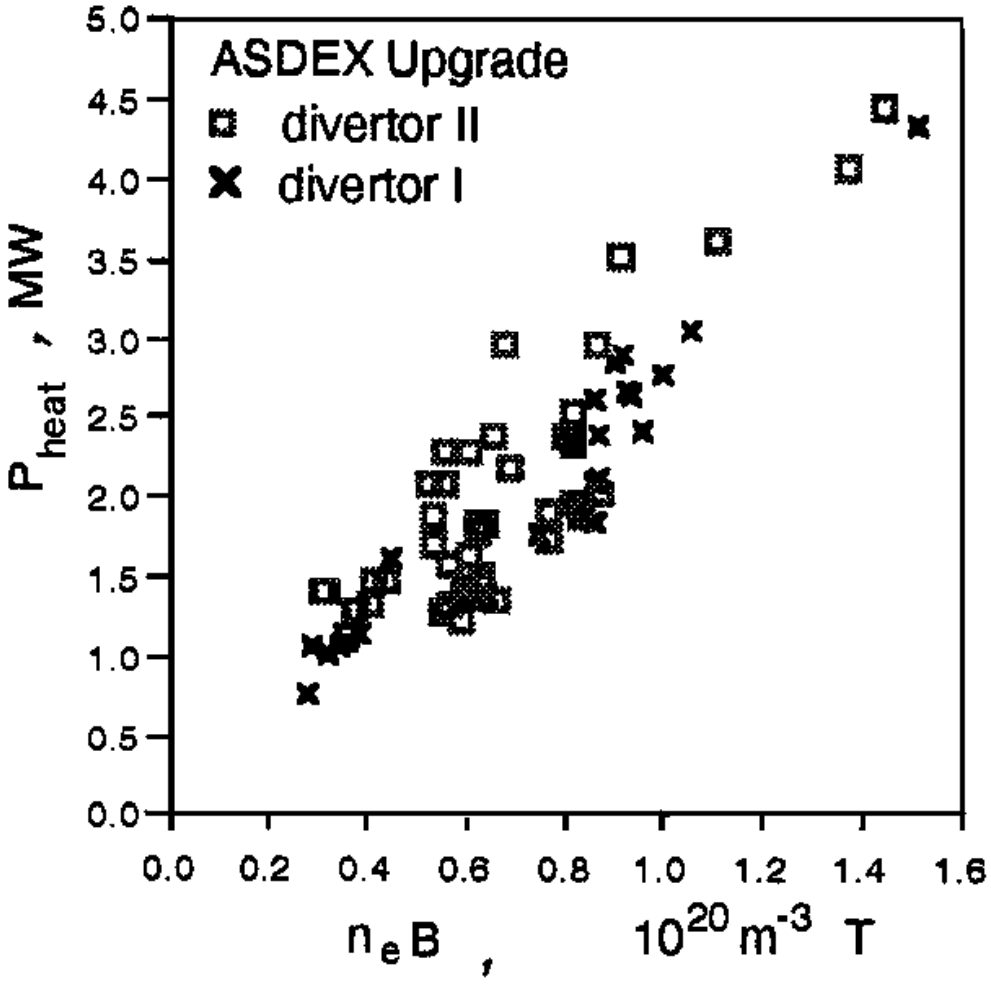

Fig.6b. H-mode power threshold in ASDEX-Upgrade against edge density (at *r-a* =2cm) multiplied by the toroidal magnetic field (Suttrop W et al 1999)

ii. Reversed magnetic field direction

The deviation of the calculated radial electric field from the neoclassical value is relatively pronounced near the separatrix in the outer midplane, Fig. 4. In the case of reversed (unfavorable) toroidal magnetic field the dip near the separatrix usually is considerably smaller (UEDGE, SOLPS5.0). In some low power regimes the radial electric field may even change its sign. The reason for this difference is connected with the contribution of the anomalous radial transport of the toroidal (parallel) momentum (Rozhansky et al 2002). The character of the parallel fluxes in the SOL is quite different for reversed magnetic field and their transport through the separatrix to the core leads to the reduction of the radial electric field and its shear with respect to the case of normal magnetic field direction.

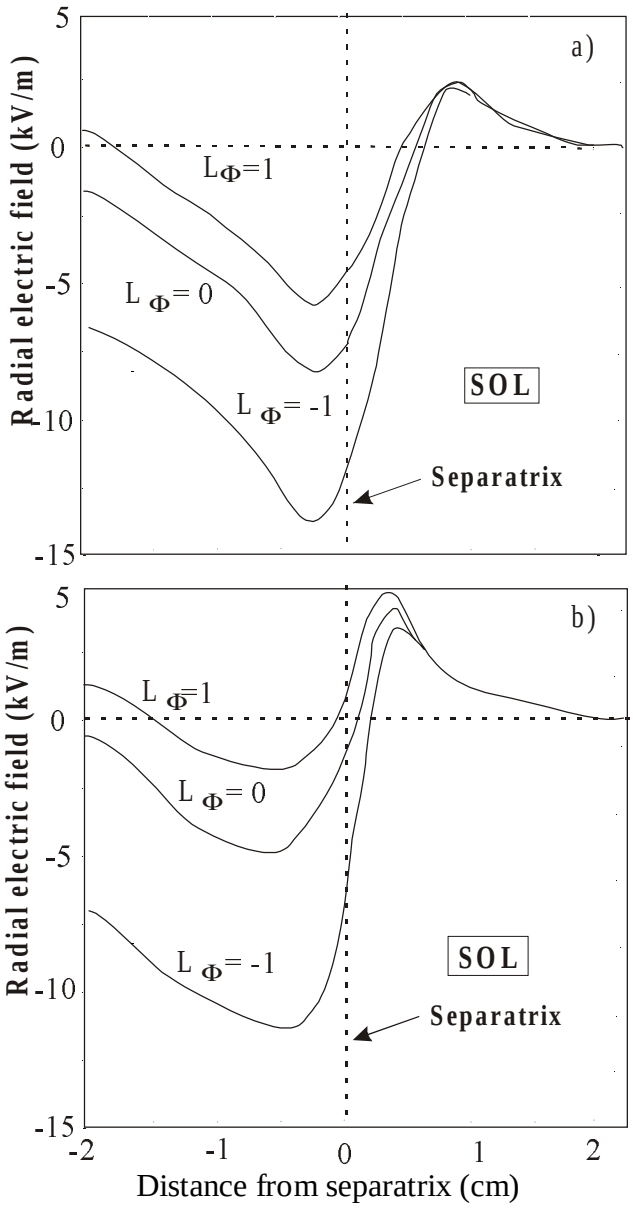

Fig.7a. Radial electric field for DIII-D calculated with UEDGE (Rognlien T et al. 1999) versus radius at the outer midplane. Frame a) –normal direction of B_z, frame b)-reversed B_z. Positive L_ϕ corresponds to the co-injection, $L_\phi = \pm 1$ corresponds to the average toroidal rotation $\pm 12 km/s$ at the inner boundary.

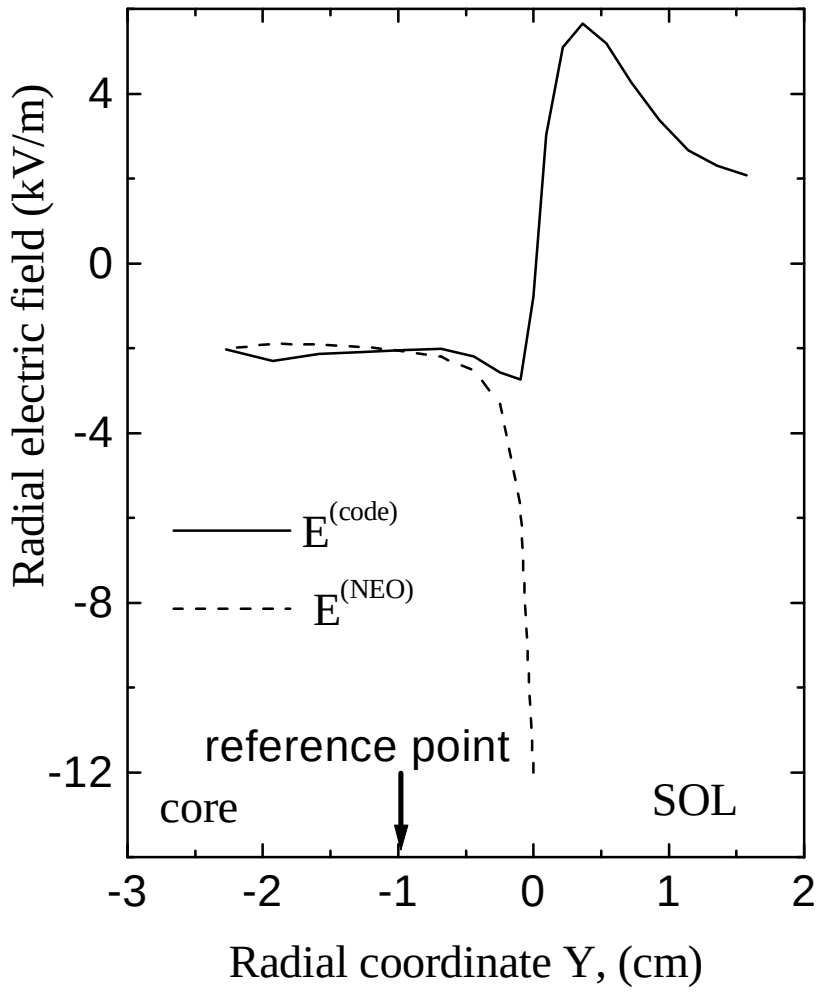

Fig7b. Radial electric field at the outer midplane calculated with B2SOLPS5.0 for ASDEX Upgrade, discharge without NBI, reversed magnetic field, n=2·10^{19} m^{-3}, T_i=98 eV in the reference point. I=1 MA, B=2 T.

iii. Pellet induced H-mode

Sinc the neoclassical expression for the radial electric field and its shear contains the density scale length L_n, one would expect reduction of the L-H transition power threshold with increase of the density gradient in the separatrix vicinity. Such experiments with injection of slow pellets, which make the density gradient steeper at the edge, were performed on Tuman-3M Askinazi L G et al. 1993, T-10 Kapralov V G et al. 1995 and DIII-D Gohil P et al. 2001. The significant reduction of the threshold has been reported in accordance with neoclassical predictions.

iv. Spherical tokamaks

The first simulations of the electric field for the spherical tokamak MAST have been performed with B2SOLPS5.0 (Rozhansky et al 2003). It was demonstrated that as for high aspect ratio tokamaks, the radial electric field is close the neoclassical value.

To explain the larger power threshold of the L-H transition further simulations are necessary. One possibility is that the power should be proportional to the full magnetic field B instead of toroidal magnetic field (Takizuka T this conference). This is consistent with the neoclassical expression for the shear.

v. Transient effects

There are several dynamic processes, which may influence the radial electric field and the power threshold for L-H transition. The processes of current ramp leads to a variation of toroidal electric field. As shown by Voskoboynikov et al 2001 the account for **electron viscosity** in the parallel momentum balance equation may change significantly the radial electric field during these processes with respect to the neoclassical value.

The rise of electric field shear at the edge may be sufficient to initiate the L-H transition. The detailed experimental investigation of these effects was performed by Askinasi et al. 2000.

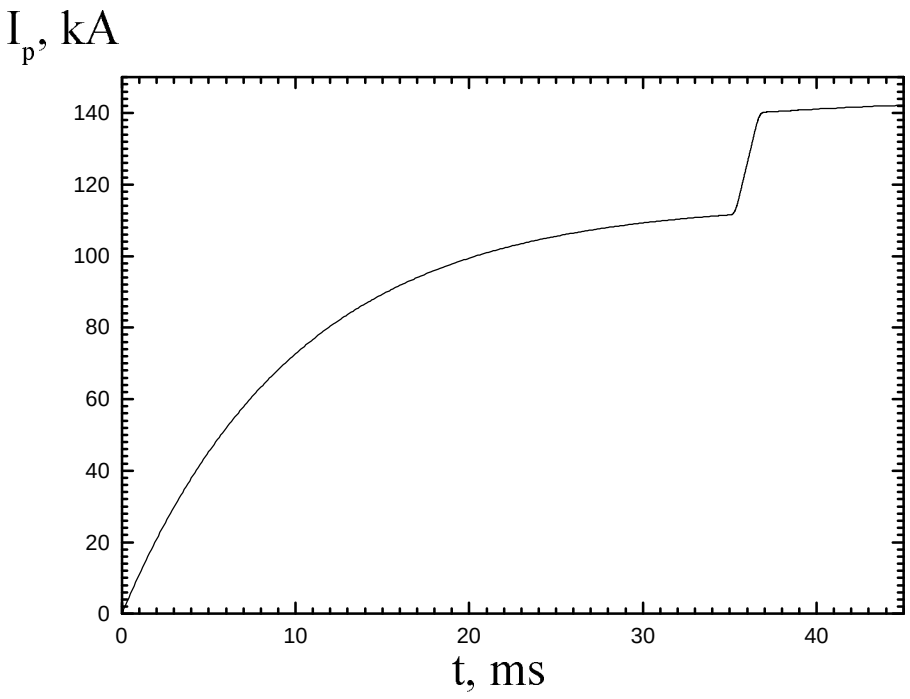

Fig.8a. Current evolution during current ramp up experiment in Tuman-3M.

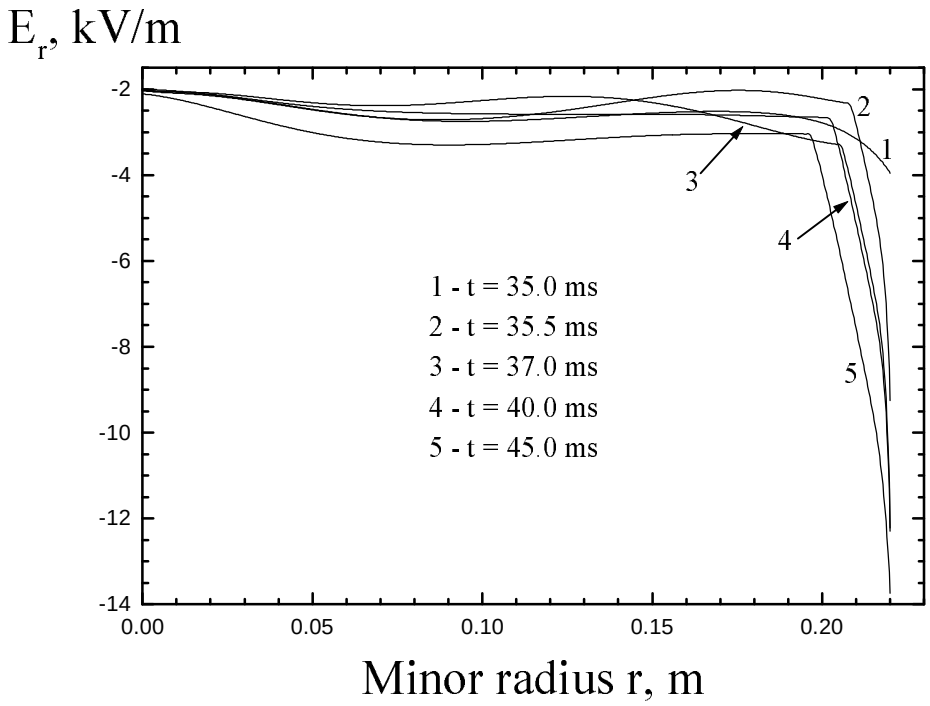

Fig.8b. Simulation of radial electric field in the Tuman-3M current ramp up experiment. Rise of radial electric field at 35.5ms is caused by the increase of toroidal electric field at the near LCFS. Further increase is connected with the barrier formation.

Modelling of L-H transition

To perform simulation of L-H transition it is necessary to have a model for the dependence of the transport coefficients on the shear of electric field. Typical dependence is given by an expression (Staebler et al 1998)

$$D / D_0 = 1/[1+\omega_s / \gamma]^n]. \qquad (10)$$

Here ω_s is the shear of $\vec{E}\times\vec{B}$ drift.

Similar dependence has been assumed in Rozhansky et al 1997, where the simulation of L-H for Tuman-3M has been performed using the transport code BATRAC. The typical equation system is

$$\frac{\partial n}{\partial t} - \frac{1}{r}\frac{\partial}{\partial r}\left[r((D(\omega_s)\frac{\partial n}{\partial r} - V(\omega_s)n)\right] = S,$$

$$\frac{3}{2}n(\frac{\partial T_{e,i}}{\partial t} + \frac{\vec{\Gamma}}{n}\nabla T_{e,i}) + nT_{e,i}\nabla\cdot\frac{\vec{\Gamma}}{n} - \frac{1}{r}\frac{\partial}{\partial r}\left[r(\frac{3}{2}n\chi_{e,i}(\omega_s))\frac{\partial T_{e,i}}{\partial r}\right] = Q_{e,i},$$

$$\frac{\partial B_\theta}{\partial t} = \frac{\partial}{\partial r}\left[\frac{1}{\mu_0\sigma_\parallel r}\frac{\partial}{\partial r}(rB_\theta)\right]. \qquad (11)$$

The shear of the $\vec{E}\times\vec{B}$ drift was calculated on the basis of the neoclassical electric field.

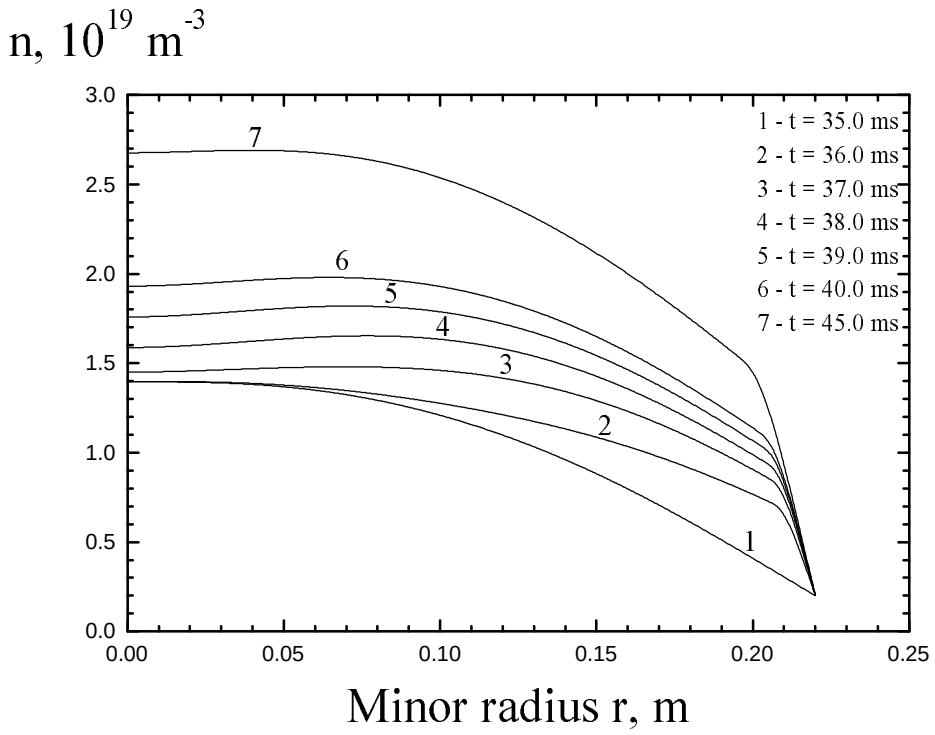

Fig.9. Simulation of density evolution during L-H transition for Tuman-3M.

The transport coefficients are strongly reduced in the barrier region of the order of 1cm near the LCFS. The width of the barrier in such models is determined by the fact that the shear inside the barrier is still large enough with respect to the critical shear:

$$T_i / e\Delta^2 \sim \omega_s , \qquad \Delta \sim \sqrt{\frac{T_i}{e\omega_s}} \tag{12}$$

where Δ is the barrier width.

A similar, but more sophisticated code has been developed by Staebler et al. 1997, and Staebler this conference (GLF2003). The equation for toroidal rotation has been added in the form

$$\frac{\partial(nm_iV_\phi)}{\partial t} - \frac{1}{r}\frac{\partial}{\partial r}\left[r\eta(\omega_s)\frac{\partial V_\phi}{\partial r}\right] = S_{m\phi}. \qquad (13)$$

Moreover, the dependence of the transport coefficients on the shear is theory based. In one version the equation for the average intensity of the ITG turbulence has been solved together with Eqs. (11), (13). The transport coefficients depend on this level, so that the equation system is closed. The results of the simulations reproduced density, temperatures and toroidal rotation evolution in the experiments with ITB formation and NBI on DIII-D. In the modern version GLF2003 the ETG mode, balloning effects and more sophisticated geometry are included. A set of gyrofluid equations that includes trapped particles is solved simultaneously.

Simulation of the H-mode

The detailed simulations of H-mode by 2D codes may contribute to the understanding of the ETB physics. A simulation of the H-mode for ASDEX Upgrade was performed recently (Rozhansky et al 2003). Transport coefficients were reduced by a factor 5 in the region 1.5mm inside and 0.5mm outside the separatrix at the equatorial midplane in accordance with experimental observations.

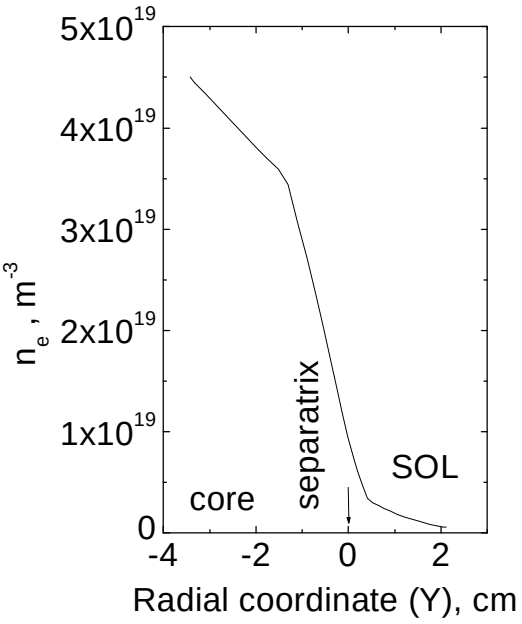

Fig.10a. Density for ASDEX Upgrade H-mode in the equatorial midplane, simulation by B2SOPLS5.0.

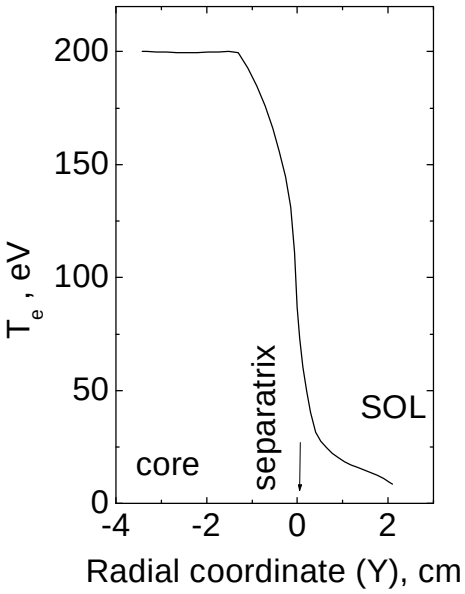

Fig.10b. Electron temperature for ASDEX Upgrade H-mode in the equatorial midplane, simulation by B2SOPLS5.0.

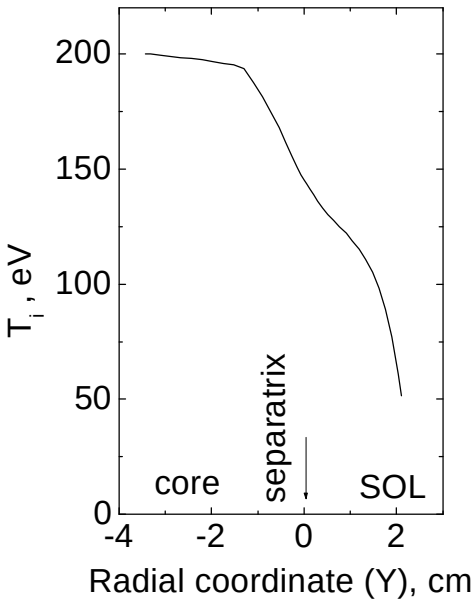

Fig.10c. Ion temperature for ASDEX Upgrade H-mode in the equatorial midplane, simulation by B2SOPLS5.0.

The steep density profile in the barrier region corresponds to the drop of the diffusion coefficient inside the barrier. The electron temperature profile also shows a barrier formation. The ion temperature profile is more gradual due to the role of neutral heat conductivity, neoclassical ion heat flux and the influence of the SOL. In the H-mode the neoclassical heat flux for ions within the barrier is of the order of anomalous heat flux (with the reduced diffusion coefficient), while for electron heat flux and particle flux the neoclassical contribution remains small.

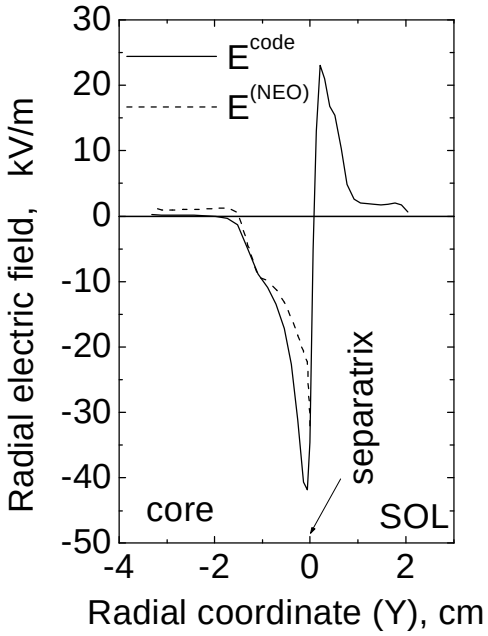

Fig.11. Radial electric field for ASDEX Upgrade H-mode in the equatorial midplane, simulation by B2SOPLS5.0.

As in the L-mode the radial electric field remains of the order of the neoclassical electric field. The absolute value is significantly larger due to the steep density gradient within the barrier.

Of special interest is the simulation of the H-mode with a fluid code coupled to a turbulence code. Such an approach is developed with UEDGE code and 3D turbulence code BOUT, Rognlien T this conference. Such a task is quite encouraging and demands huge computational resources. At present it is possible to couple only density and temperature, however the full self-consistent approach is under development.

Simulations of ELMs

Analytical model for type I ELMy H-mode based on linear ballooning mode theory has been recently put forward by J.-S. Lönnroth et al this conference. It is assumed that the balloning modes are controlled by the pressure gradient. The first term in the linear differential equation represents the growth rate of the ballooning mode amplitude ξ and the second one the level of background thermal fluctuations.

$$\frac{d\xi}{dt} = C_1 \frac{c_s}{\sqrt{L_p R}}\left(1-\frac{\alpha_c}{\alpha}\right)H\left(1-\frac{\alpha_c}{\alpha}\right)\xi - C_2 \frac{c_s}{R}(\xi-\xi_0)$$

$$H(x)=\begin{cases}0, x<0\\ 1, x\geq 0\end{cases} \qquad c_{s,i}=\sqrt{\frac{T_e}{m_i}} \qquad L_{p,j}=\frac{p}{\nabla p}$$

$$C_1 \approx 1 \qquad C_2 \approx 0.1 \qquad \xi_0 \approx 0.01$$

The analytical linear ballooning model has been implemented into the JETTO transport code. The ELM model based on linear ballooning stability theory can reproduce the experimental dynamics of type I ELMy H-mode when coupled to a transport simulation.

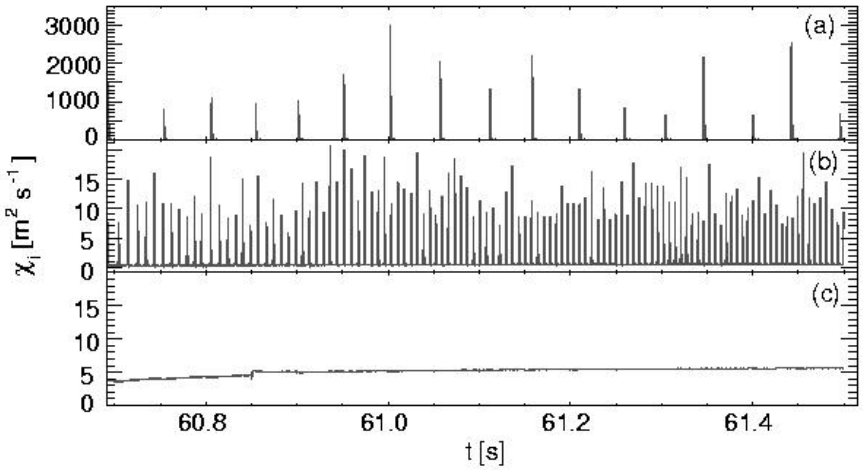

From ETB towards ITB

The codes of the type of GLF2003 may be successively used for ITB simulation. The main physical issue here is the same as for the ETBs: the formation of strong shear of poloidal $\vec{E}\times\vec{B}$ drift, which may be initiated by the rise of temperatures or density gradients, or change in the contribution of the toroidal rotaion etc.

In the formation if an ITB there is an additional special feature: there are several experimental indications that ITB's are associated with **rational flux surfaces with low *q* values**. Radial electric fields in the vicinity of the magnetic island might be perturbed and the corresponding change of the poloidal drift shear might create a seed for the ITB formation.

Models:

i. Formation of the current of fast ions during the fishbone activity, Guenter S *et al* 2001

ii. Modified radial electric field in the vicinity of an island Shaing 2001, 2002 (without toroidal rotation and anomalous viscosity).

iii. Viscous shear layer, where radial electric field changes from the neoclassical value outside the island to a different value inside the island (zero for non-rotating islands) similar to the situation in the vicinity of a separatrix at the edge (Kaveeva et al 2003)

Simulations of electric field near the magnetic islands are necessary. A first step was made by X Bonnin et al 2001.

Summary

Simulations of the radial electric field by several fluid and Monte Carlo codes demonstrate that radial electric field in the separatrix vicinity is close to the neoclassical value. No bifurcation has been observed during the simulations. The neoclassical character of the electric field is consistent with existing scaling for L-H transition. Several features observed in the experiments, such as dependence of the threshold on the toroidal magnetic field direction, pellet induced L-H transition etc may be explained on the basis of simulation results. Possible triggering of ITB's formation by the magnetic islands at rational flux surfaces deserves future modeling. One-dimensional transport codes with transport coefficients depending on the poloidal $\vec{E}\times\vec{B}$ drift shear might be an adequate tool for simulation of both ITB and ETB formation and evolution.